Resonance contributions to the electron-impact excitation of ions in the distorted-wave approximation

M. S. Pindzola
Department of Physics, Auburn University, Auburn, Alabama 36849-3501

D. C. Griffin
Department of Physics, Rollins College, Winter Park, Florida 32789

C. Bottcher
Physics Division, Oak Ridge National Laboratory, Oak Ridge, Tennessee 37830
(Received 29 April 1985)

In analogy with recent work on dielectronic recombination, an average-configuration distorted-wave method is developed to calculate resonance structures in the electron excitation of ions. Confirming previous results, large resonance contributions are found for the $2s \rightarrow 3s$ and $2p \rightarrow 3s$ excitations of O^{5+}. Large resonance contributions are also found for the $2p^6 \rightarrow 2p^5 3s$ excitation of Ti^{12+}. Radiative-coupling and electric-field-mixing effects are discussed.

I. INTRODUCTION

Electron-ion scattering processes play a key role in the understanding of many types of high-temperature plasmas. Excitation, ionization, and recombination cross sections may be strongly influenced by the presence of autoionizing levels within a highly ionized atom.[1] Even in simple heliumlike ions[2] ground-state excitation collision rates at certain temperatures may be enhanced by a factor of 2 due to autoionizing resonances. Early predictions[3] of large resonance enhancements in the excitation cross sections of lithiumlike ions have been confirmed by recent close-coupling and distorted-wave calculations.[4,5] Although the lithiumlike ions are perhaps the best studied experimentally,[6] the only specific measurements are on the $2s \rightarrow 2p$ excitation which is not predicted to have and does not show any resonance enhancement.

An indirect check on the various theoretical methods of calculating the effects of resonances in electron-impact excitation is provided by recent dielectronic-recombination cross-section measurements.[7,8] The dielectronic recombination process may be thought of as resonant recombination into an autoionizing level followed by radiative decay. The indirect-excitation process may be thought of as resonant recombination into an autoionizing level followed by an autoionizing decay. Theoretical methods[9–13] based on the direct computation of energies and wave functions of the many autoionizing levels, followed by distorted-wave calculation of autoionizing rates and resonant-recombination cross sections, have proved quite successful in describing the dielectronic recombination process. In this paper we apply the same methods to the calculation of those electron-impact excitation cross sections where resonance enhancements are believed to be strong. One of the nice features of this approach is that one focuses on the identification of possible autoionizing levels, their relative position in energy, and their possible paths of radiative or autoionizing decay. In this way it serves to complement those theoretical methods which either directly calculate the collision scattering matrix in the presence of closed channels[14] or analytically continue the known S matrix below threshold.[15]

In Sec. II we review the calculational method and discuss the average-configuration indirect excitation cross section. In Sec. III we apply the method to the calculation of the $2s \rightarrow 3s$ and $2p \rightarrow 3s$ excitation cross sections in lithiumlike oxygen. Comparison is then made with previous theoretical calculations.[3–5] In Sec. IV we calculate the $2p^6 \rightarrow 2p^5 3s$ excitation cross section in neonlike titanium. The same transition in neonlike iron has been predicted to have a large resonance enhancement near threshold.[16] These results should be of interest to those researchers[17,18] who model neonlike excitation schemes for the production of soft-x-ray superfluorescence.[19] In Sec. V we give a short conclusion.

II. CALCULATIONAL METHODS

In the independent processes approximation, the total electron-impact excitation cross section from a state of level i to all states of level f is given by

$$\sigma_t(i \rightarrow f) = \sigma_{dx}(i \rightarrow f) + \sigma_{ix}(i \rightarrow f) , \tag{1}$$

where $\sigma_{dx}(i \rightarrow f)$ is the direct excitation cross section and $\sigma_{ix}(i \rightarrow f)$ is the indirect excitation cross section due to resonant processes. The indirect section is given by

$$\sigma_{ix}(i \rightarrow f) = \sum_j \sigma_r(i \rightarrow j) B_a(j \rightarrow f) , \tag{2}$$

where $\sigma_r(i \rightarrow j)$ is the resonant-recombination cross section from a state of level i to all states of the autoionizing level j. The branching ratio for autoionization from a state of level j to all states of level f is given by

$$B_a(j\rightarrow f)=\frac{A_a(j\rightarrow f)}{\sum_m A_a(j\rightarrow m)+\sum_n A_r(j\rightarrow n)}\ , \tag{3}$$

where $A_a(j\rightarrow m)$ is the autoionization rate to all states m which lie below j, including levels i and f, and $A_r(j\rightarrow n)$ is the radiative rate to all states n which lie below j.

The general cross section expression of Eq. (1), and the corresponding transition rates, may be evaluated in any pure or intermediate coupling scheme. However, in complex configurations it may be next to impossible to carry out a level to level calculation of the total cross section because of the very large number of levels involved. Thus when performing survey calculations for a variety of atomic ions, it is useful to develop a method which dramatically reduces the number of individual rates which must be calculated.

The direct excitation cross section may be calculated in an average-configuration distorted-wave approximation.[20] Consider the following transition between configurations

$$(n_l l_1)^{q_1}(n_2 l_2)^{q_2} k_i l_i \rightarrow (n_1 l_1)^{q_1-1}(n_2 l_2)^{q_2+1} k_f l_f\ , \tag{4}$$

where n_i is the principal quantum number, l_i is the angular-momentum quantum number, q_i is the occupation number, and k_i is the linear-momentum wave number. The average-configuration direct excitation cross section from configuration I to configuration F is given by (in atomic units)

$$\begin{aligned}\bar{\sigma}_{dx}(I\rightarrow F)=\frac{8\pi q_1(4l_2+2-q_2)}{k_i^3 k_f}\sum_{l_i}\sum_{l_f}(2l_i+1)(2l_f+1)\\ \times\Bigg[\sum_\lambda a(l_1,l_i,l_2,l_f,\lambda)[R^\lambda(n_2l_2,k_fl_f;n_1l_1,k_il_i)]^2\\ +\sum_{\lambda'} b(l_1,l_i,l_2,l_f,\lambda')[R^{\lambda'}(k_fl_f,n_2l_2;n_1l_1,k_il_i)]^2\\ -\sum_\lambda\sum_{\lambda'} c(l_1,l_i,l_2,l_f,\lambda,\lambda')R^\lambda(n_2l_2,k_fl_f;n_1l_1,k_il_i)R^{\lambda'}(k_fl_f,n_2l_2;n_1l_1,k_il_i)\Bigg]\ ,\end{aligned} \tag{5}$$

where $R^\lambda(ij;rt)$ is the usual Slater radial integral for the Coulomb interaction between electrons and the angular coefficients a, b, and c may be expressed in terms of standard 3-j and 6-j symbols, as found in previous work.[13] The continuum normalization is chosen as one times a sine function.

In analogy with recent work on dielectronic recombination,[13] one may also calculate the indirect excitation cross section in an average-configuration distorted-wave approximation. Using the isolated resonance approximation and the principle of detailed balance, the resonant-recombination cross section is given by

$$\sigma_r(i\rightarrow j)=\frac{2\pi^2}{\Delta\varepsilon\, k_i^2}\frac{g_j}{2g_i}A_a(j\rightarrow i)\ , \tag{6}$$

where $\Delta\varepsilon$ is an energy bin width larger than the largest resonance width and g_i is the statistical weight of level i. Combining Eqs. (2), (3), and (6), the average-configuration indirect excitation cross section from configuration I to configuration F through configuration J, is defined by

$$\begin{aligned}&\bar{\sigma}_{ix}(I\rightarrow F)\\ &=\frac{2\pi^2}{\Delta\varepsilon\, k_i^2}\frac{1}{2G_I}\sum_j g_j\frac{\sum_i A_a(j\rightarrow i)\sum_f A_a(j\rightarrow f)}{\sum_m A_a(j\rightarrow m)+\sum_n A_r(j\rightarrow n)}\ ,\end{aligned} \tag{7}$$

where G_I is the statistical weight of configuration I. Equation (7) can be greatly simplified in two limiting cases. If $\sum_f A_a(j\rightarrow f)$ is much greater than the sum over all other autoionization and radiative decay channels, which is typically the case, then Eq. (7) becomes

$$\bar{\sigma}_{ix}(I\rightarrow F)\approx\frac{2\pi^2}{\Delta\varepsilon\, k_i^2}\frac{G_J}{2G_I}\bar{A}_a(J\rightarrow I)\ , \tag{8}$$

where the average-configuration autoionizing rate from configuration J to configuration I is given by

$$\bar{A}_a(J\rightarrow I)=\frac{1}{G_J}\sum_j g_j\sum_i A_a(j\rightarrow i)\ . \tag{9}$$

On the other hand if $\sum_i A_a(j\rightarrow i)$ is much greater than the sum over all other autoionization and radiative decay channels, then Eq. (7) becomes

$$\bar{\sigma}_{ix}(I\rightarrow F)\approx\frac{2\pi^2}{\Delta\varepsilon\, k_i^2}\frac{G_J}{2G_I}\bar{A}_a(J\rightarrow F)\ . \tag{10}$$

The working equation for the average-configuration indirect excitation cross section is an interpolation between these two limiting cases:

$$\bar{\sigma}_{ix}(I\rightarrow F)=\frac{2\pi^2}{\Delta\varepsilon\, k_i^2}\frac{G_J}{2G_I}\frac{\bar{A}_a(J\rightarrow I)\bar{A}_a(J\rightarrow F)}{\sum_M \bar{A}_a(J\rightarrow M)+\sum_N \bar{A}_r(J\rightarrow N)}\ , \tag{11}$$

where $\bar{A}_r(J\rightarrow N)$ is the average-configuration radiative rate. Explicit expressions for the average-configuration rates $\bar{A}_a$ and $\bar{A}_r$ in terms of Slater and dipole radial integrals are found in a previous work.[13]

A variety of calculational programs were used to generate the average-configuration cross sections of Eqs. (5) and (11) for a particular atomic ion. The bound-state energies and atomic orbitals for the many configurations needed to evaluate a total excitation cross section are generated using the radial wave function code developed by Cowan.[21] These bound radial wave functions are solutions to the Hartree-Fock equations with relativistic modifications, which include the mass-velocity and Darwin corrections within modified differential equations.[22] The continuum radial wave functions are calculated using a local semiclassical approximation for the exchange interaction.[23] This exchange term simplifies the solution of the differential equation and generally gives results in close agreement with results obtained from a full non-local Hartree-Fock continuum calculation. Relativistic effects are also included in the distorted-wave continuum wave functions by the addition of a local mass-velocity potential.

III. RESULTS FOR LITHIUMLIKE OXYGEN

To test the average-configuration approximation and our numerical methods, we first calculated the $2s\rightarrow 3s$ and $2p\rightarrow 3s$ excitations in lithiumlike oxygen. Direct excitation cross section results for several transitions in O^{5+}, obtained using Eq. (5), are given in Table I(a). Our distorted-wave results are in good agreement with the distorted-wave results of Mann,[24] and in fair agreement with the close-coupling results of Bhadra and Henry.[4] Based on a comparison of excitation collision cross sections, one might suspect that the relatively weak $2p\rightarrow 3s$ transition might be strongly influenced by autoionization states found below the $3p$ and $3d$ thresholds.

The energies of several autoionizing configurations in O^{4+}, obtained using Cowan's wave function code,[21] are shown in Fig. 1. The energies are calculated relative to the $1s^2 3s$ configuration of O^{5+}. For the autoionizing configurations converging to the $3p$ and $3d$ thresholds, only the lowest angular momentum state of a given $3pnl$ or $3dnl$ set of configurations is shown; while all the con-

TABLE I. O^{5+} excitation cross sections near threshold. (a) Shows nonresonant cross sections. (b) Shows total cross sections including only $3pnl$ and $3dnl$ configurations. (c) Shows total cross sections.

(a)

Excitation	Average-configuration distorted wave	Close coupling (Ref. 4)	Distorted wave (Ref. 24)	Green's function (Ref. 3)
$2s\rightarrow 3s$	1.58 Mb[a]	1.27 Mb	1.51 Mb	1.76 Mb
$2s\rightarrow 3p$	0.62 Mb	0.93 Mb	0.59 Mb	
$2s\rightarrow 3d$	2.35 Mb	2.13 Mb	2.36 Mb	
$2p\rightarrow 3s$	0.19 Mb	0.36 Mb	0.15 Mb	0.34 Mb
$2p\rightarrow 3p$	2.86 Mb	1.50 Mb	2.76 Mb	
$2p\rightarrow 3d$	6.96 Mb	5.09 Mb	7.06 Mb	

(b)

Excitation	Average-configuration distorted wave	Close coupling (Ref. 4)	Close coupling (Ref. 5)	Distorted wave (Ref. 5)
$2s\rightarrow 3s$	3.03 Mb	2.68 Mb	2.70 Mb	2.77 Mb
$2p\rightarrow 3s$	4.70 Mb	2.62 Mb	3.48 Mb	3.30 Mb

(c)

Excitation	Average configuration distorted wave	Green's function (Ref. 3)
$2s\rightarrow 3s$	3.94 Mb	3.46 Mb
$2p\rightarrow 3s$	5.38 Mb	10.9 Mb

[a] 1 Mb $=1.0\times 10^{-18}$ cm^2.

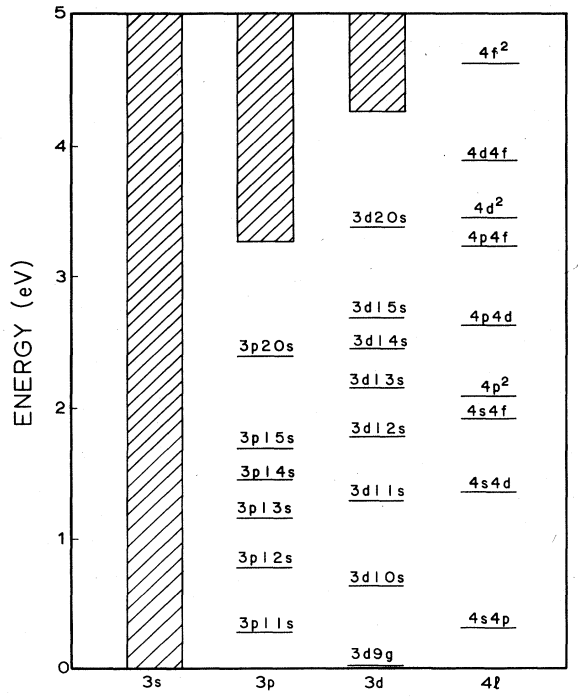

FIG. 1. Energy-level diagram for autoionizing configurations of O^{4+}. All energies are relative to the $1s^2 3s$ configuration of O^{5+}.

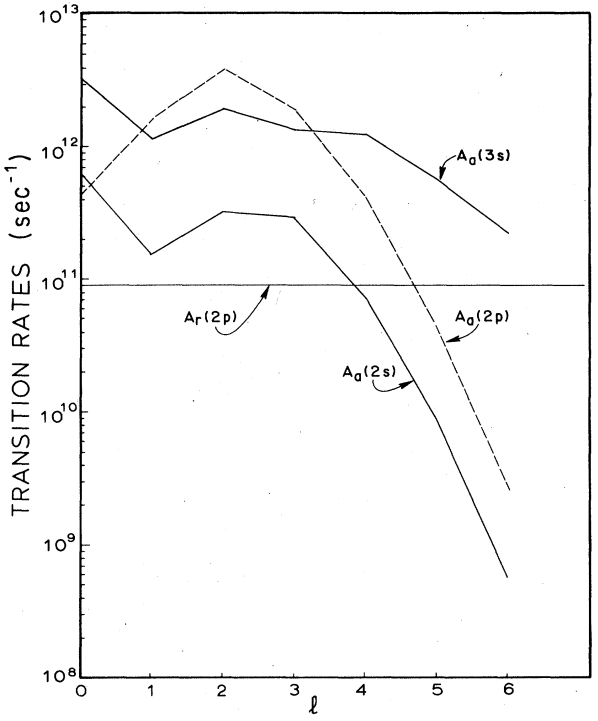

FIG. 2. Autoionization and radiative rates for the $3d\,10l$ configurations of O^{4+}. The label $A_a(nl')$ refers to the autoionizing transition $3d\,10l \rightarrow nl' + e^-$. The label $A_r(2p)$ refers to the radiative transition $3d\,10l \rightarrow 2p\,10l + h\nu$.

figurations converging to $4l$ thresholds, in this energy range, are shown. More accurate calculations are needed to determine the precise position of $3d\,9l$ configurations relative to the $3s$ threshold.

We first concentrate on the autoionizing configurations converging to the $3d$ threshold, since they make the largest contribution to the O^{5+} indirect $2s \rightarrow 3s$ and $2p \rightarrow 3s$ excitation cross sections, obtained using Eq. (11). For the $3dnl$ configurations explicit autoionization and radiative rates were calculated for $n \leq 21$ and $l \leq 6$. For higher values of n, $\overline{A}_a$ goes approximately as $1/n^3$, while $\overline{A}_r$ is nearly a constant. We extrapolated the autoionization rates to high values of n by fitting the calculated values of $n^3\overline{A}_a$ to the formula $A + B/n^2 + C/n^4$. For higher values of l, $\overline{A}_a$ was calculated using hydrogenic wave functions while $\overline{A}_r$ is again nearly a constant. For $n \leq 18$ the $3dnl$ configurations can autoionize to the $2s$, $2p$, and $3s$ configurations of O^{5+}. For $n \geq 19$ the $3dnl$ configurations can also autoionize to the $3p$ configuration of O^{5+}. When available the $3p$ decay rate is usually an order of magnitude greater than the other three channels combined.

In calculating radiative rates we must distinguish between two types of radiative transitions. The first type includes those in which the Rydberg electron is a spectator; for example, transitions of the form $3dnl \rightarrow 2pnl + h\nu$ or $3dnl \rightarrow 3pnl + h\nu$. We ignore cascade effects by leaving out radiative transitions to $3pnl$ configurations for which $n \geq 11$. In the second type the Rydberg electron is the active electron; for example, transitions of the form $3dnl \rightarrow 3dn'l'$. For O^{5+} second type transitions are not very significant, but in atomic ions at higher stages of ionization they prove quite important.[25]

Autoionization and radiative rates for the $3d\,10l$ configurations of O^{4+}, calculated in the average-configuration distorted-wave approximation, are shown in Fig. 2. This type of figure has been used before to explain various aspects of the dielectronic recombination process.[25] Consider first the $2s \rightarrow 3s$ indirect excitation ignoring autoionization to the $2p$ configuration. In this case the conditions leading to Eq. (8) are quite well satisfied and the $2s \rightarrow 3s$ cross section is governed by the lower $2s$ decay rate. Even with the $2p$ decay rate included we expect the $2s \rightarrow 3s$ cross section calculated from Eq. (11) to be fairly accurate. On the other hand consider the $2p \rightarrow 3s$ indirect excitation ignoring the $2s$ decay rate. Since the $3s$ and $2p$ decay rates are of similar magnitude, we do not expect that the average cross section of Eq. (11) to be as accurate for this case. Based on previous work,[13] we suspect that Eq. (11) will tend to overestimate the true $2p \rightarrow 3s$ indirect cross section.

The total cross sections for the $2s \rightarrow 3s$ and $2p \rightarrow 3s$ excitation of O^{5+}, obtained using Eqs. (5) and (11), are shown in Figs. 3 and 4, respectively. Resonance contributions from the $3pnl$, $3dnl$, and $4l4l'$ configurations are included. The slowly oscillating theoretical curves were obtained by convoluting the spectrum of narrow resonance peaks generated by our computer codes with a Gaussian

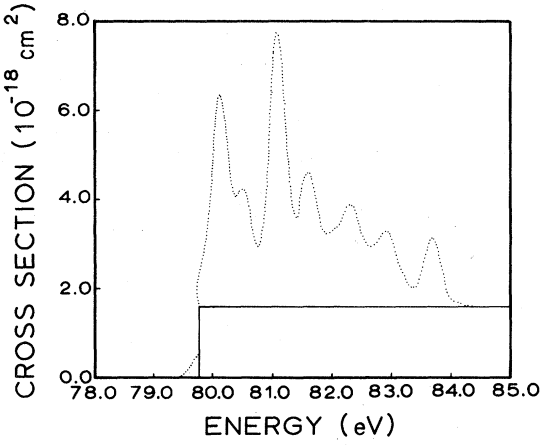

FIG. 3. Electron-impact $2s \rightarrow 3s$ excitation cross section of O^{5+}. The solid curve is the direct excitation cross section, while the dotted curve is the sum of the direct and indirect cross sections.

energy distribution with a full width at half maximum equal to 0.3 eV. Electron energy distributions in crossed-beam experiments typically have an energy width of this magnitude.[6] In Fig. 3 the first peak in the spectrum at 80.1 eV is from the $4s\,4p$ configuration, the shoulder at 80.5 eV is from the $3d\,10l$ configurations, and the largest peak at 81.1 eV is from the $4s\,4d$ configuration. In Fig. 4 the first peak in the spectrum at 68.1 eV is from the $3p\,11l$ and $4s\,4p$ configurations, the next peak at 68.5 eV is from the $3d\,10l$ configurations, and the largest peak at 70.2 eV is from the $4p\,4d$ configuration.

In order to compare our total cross section results for O^{5+} with previous theoretical calculations, we make a simple average of the slowly oscillating curves of Figs. 3 and 4 over the energy range from the $3s$ to $3p$ thresholds. For comparison with previous distorted-wave and close-coupling calculations, our results in Table I(b) only include contributions from the $3pnl$ and $3dnl$ autoionizing configurations. The average-configuration distorted-wave results for the $2s \rightarrow 3s$ excitations are 9% to 13% higher than previous calculations,[4,5] while the $2p \rightarrow 3s$ excitation results are 35% to 79% higher than previous work.[4,5] We note that the close-coupling calculation of Clark *et al.*[5] is 33% higher than the close-coupling calculation of Bhadra and Henry[4] for the $2p \rightarrow 3s$ excitation. Since the Green's function calculations of Presnyakov and Urnov[3] did include the configurations converging to the $4l$ thresholds, a separate comparison is made in Table I(c). The $2s \rightarrow 3s$ distorted-wave results are about 14% higher than the previous calculation,[3] while the $2p \rightarrow 3s$ excitation results are 51% lower than previous work.[3] It can be concluded from all of these calculations of lithiumlike oxygen that large resonance enhancements are present in the $2s \rightarrow 3s$ and $2p \rightarrow 3s$ excitations and that our study indicates that the average-configuration distorted-wave method should yield an accuracy of better than a factor of 2 in predicting the average total cross section.

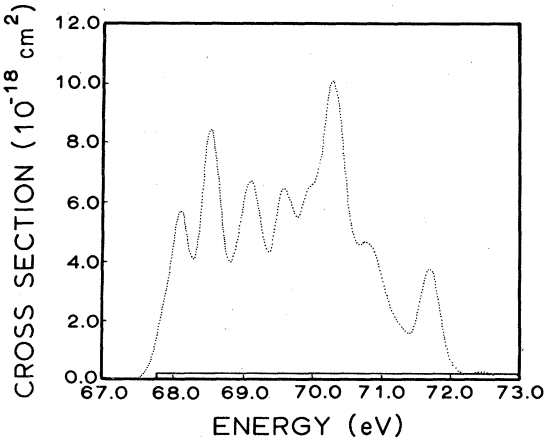

FIG. 4. Electron-impact $2p \rightarrow 3s$ excitation cross section of O^{5+}. The solid curve is the direct excitation cross section, while the dotted curve is the sum of the direct and indirect cross sections.

IV. RESULTS FOR NEONLIKE TITANIUM

Direct excitation cross section results for several transitions in Ti^{12+}, obtained using Eq. (5), are given in Table II(a). Based on a comparison of excitation collision cross sections, one might suspect that the relatively weak $2p^6 \rightarrow 2p^5 3s$ transition is strongly influenced by autoionization states found below the $2p^5 3p$ and $2p^5 3d$ thresholds. The energies of several autoionizing configurations in Ti^{11+}, obtained using Cowan's wave function code,[21] are shown in Fig. 5. More accurate calculations are needed to determine the precise position of the $2p^5 3p\,9l$ and $2p^5 3d\,6l$ configurations relative to the $2p^5 3s$ threshold.

Autoionization and radiative rates for the $2p^5 3d\,7l$ configurations of Ti^{11+}, calculated in the average-configuration distorted-wave approximation, are shown in Fig. 6. For calculation of the $2p^6 \rightarrow 2p^5 3s$ indirect cross section, conditions leading to Eq. (8) are extremely well satisfied. We thus expect that the average-configuration cross section for the $2p^6 \rightarrow 2p^5 3s$ excitation of Ti^{12+} to be more accurate than either of the excitations considered for O^{5+} in Sec. III. The total cross section for the

TABLE II. Ti^{12+} excitation cross sections near threshold. (a) Shows nonresonant cross sections. (b) Shows total cross section.

(a)

Excitation	Distorted wave
$2p^6 \rightarrow 2p^5 3s$	0.017 Mb[a]
$2p^6 \rightarrow 2p^5 3p$	0.256 Mb
$2p^6 \rightarrow 2p^5 3d$	0.491 Mb

(b)

Excitation	Distorted wave
$2p^6 \rightarrow 2p^5 3s$	0.736 Mb

[a] 1 Mb $= 1.0 \times 10^{-18}$ cm^2.

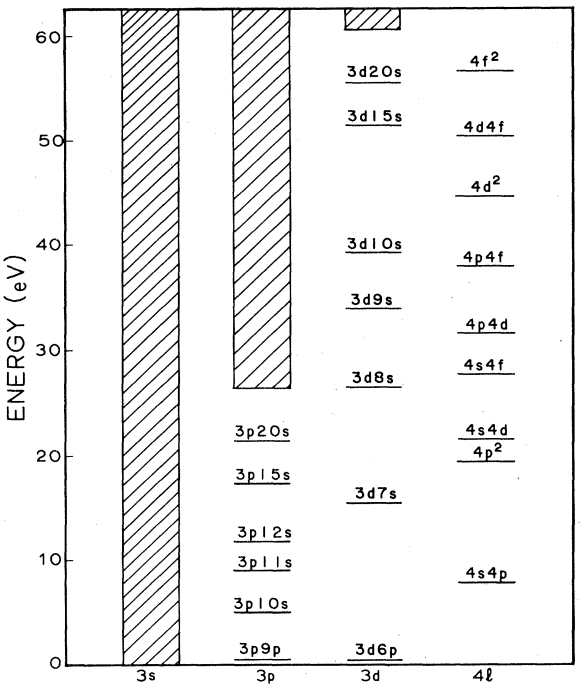

FIG. 5. Energy level diagram for autoionizing configurations of Ti^{11+}. All energies are relative to the $1s^22s^22p^53s$ configuration of Ti^{12+}.

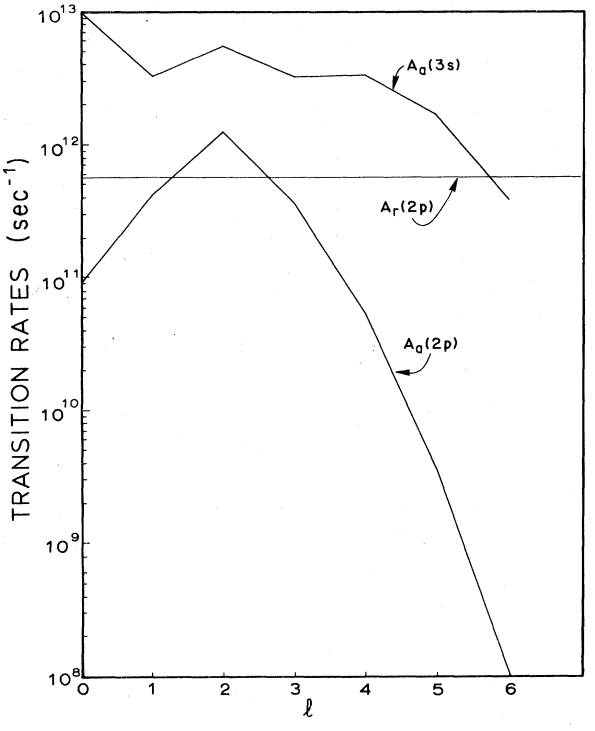

FIG. 6. Autoionization and radiative rates for the $2p^53d\,7l$ configurations of Ti^{11+}. The label $A_a(2p)$ refers to the autoionizing transition $2p^53d\,7l \rightarrow 2p^6 + e^-$. The label $A_a(3s)$ refers to the autoionizing transition $2p^53d\,7l \rightarrow 2p^53s + e^-$. The label $A_r(2p)$ refers to the radiative transition $2p^53d\,7l \rightarrow 2p^67l + h\nu$.

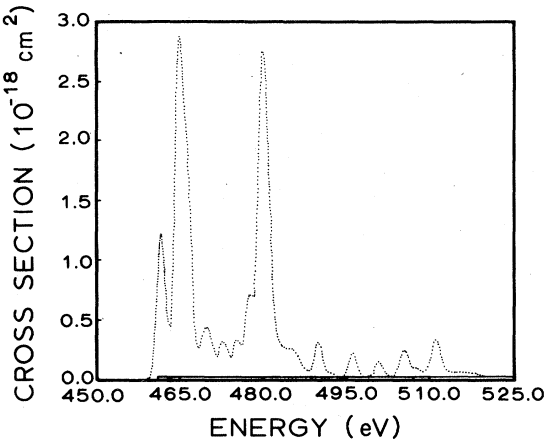

FIG. 7. Electron-impact $2p^6 \rightarrow 2p^53s$ excitation cross section of Ti^{12+}. The solid curve is the direct excitation cross section, while the dotted curve is the sum of the direct and indirect cross sections.

$2p^6 \rightarrow 2p^53s$ excitation of Ti^{12+} is shown in Fig. 7. Resonance contributions from the $2p^53pnl$, $2p^53dnl$, and $2p^54l\,4l'$ configurations are included. A full width at half maximum equal to 1.5 eV is used to convolute the narrow resonance spectrum. The large peak at 465 eV in the $2p^6 \rightarrow 2p^53s$ cross section of Fig. 7 is from the $2p^53d\,6l$ configurations. The equally large peak at 480 eV is from the $2p^53d\,7l$ configurations.

Our total cross section results for Ti^{12+} are given in Table II(b). The average cross section near threshold is a factor of 40 times the direct nonresonant cross section. Collision rate coefficients for the $2p^6 \rightarrow 2p^53s$ excitation of Ti^{12+} are given in Table III. The abundance of the neonlike ionization stage of Ti is expected to be highest for the electron temperatures chosen. At the lowest temperature the rate coefficient is enhanced by a factor of 6 while at the highest temperature the rate coefficient moves up by a factor of 3.

Recent dielectronic recombination cross section measurements[7,8] have sparked renewed interest in the effects of external electric fields on electron-ion scattering processes.[10,25] Using Fig. 6 one can make a qualitative argument in regard to the effect external electric fields will have on the indirect excitation cross section of Ti^{12+}. For all values l of the $2p^53d\,7l$ configuration, the $2p^6$ autoionization decay rate, which governs the cross section, lies below the $2p^53s$ decay rate. This remains true for all $2p^53dnl$ configurations with $n > 7$. Thus Stark field mixing of the levels of each of the $2p^53dnl$ configurations will change the shape of the autoionization rate curves as a function of l, but cannot change the fact that the $2p^6$ decay rates are smaller than the $2p^53s$ decay rates. We thus expect that the effect of external fields on the $2p^6 \rightarrow 2p^53s$ excitation cross section in Ti^{12+} is quite small. In fact for most electron-ion excitation cross sections we expect that external electric fields will have a negligible effect on the average total cross section.

V. CONCLUSIONS

We have shown that the calculation of electron-impact excitation cross sections in the average-configuration

TABLE III. $Ti^{12+}2p^6 \rightarrow 2p^5 3s$ collision rates.

Temperature	Nonresonant collision rate	Total collision rate
2.29×10^6 K	3.6×10^{-12} cm^3/sec	2.5×10^{-11} cm^3/sec
4.57×10^6 K	8.2×10^{-12} cm^3/sec	3.4×10^{-11} cm^3/sec
6.86×10^6 K	9.9×10^{-12} cm^3/sec	3.0×10^{-11} cm^3/sec

distorted-wave approximation can prove quite useful in estimating resonance enhancement effects. We plan to extend our survey calculations to other atomic ions where resonance effects are expected to be important. These average-configuration calculations will also provide a guide in developing more detailed computational methods based on intermediate-coupled level to level excitation cross sections. We hope that both the survey and detailed methods will prove useful to those researchers examining the radiative output of high temperature plasmas.

ACKNOWLEDGMENTS

We wish to thank R. D. Cowan for making his atomic-structure programs available to us. We would like to thank R. J. W. Henry, A. L. Merts, J. B. Mann, L. A. Collins, and R. E. H. Clark for several useful discussions. This research was supported by the Office of Fusion Energy, U.S. Department of Energy, under Contract No. DE-AC05-84OR21400 with Martin Marietta Energy Systems, Inc.

[1]R. D. Cowan, Phys. Scr. **T3**, 200 (1983).
[2]S. S. Tayal and A. E. Kingston, J. Phys. B **17**, 1383 (1984).
[3]L. P. Presnyakov and A. M. Urnov, J. Phys. B **8**, 1280 (1975).
[4]K. Bhadra and R. J. W. Henry, Phys. Rev. A **26**, 1848 (1982).
[5]R. E. H. Clark, A. L. Merts, J. B. Mann, and L. A. Collins, Phys. Rev. A **27**, 1812 (1983).
[6]D. H. Crandall, in *Physics of Ion-Ion and Electron-Ion Collisions,* edited by F. Brouillard and J. W. McGowan (Plenum, New York, 1983), p. 201.
[7]D. S. Belic, G. H. Dunn, T. J. Morgan, D. W. Mueller, and C. Timmer, Phys. Rev. Lett. **50**, 339 (1983).
[8]P. F. Dittner, S. Data, P. D. Miller, C. D. Moak, P. H. Stelson, C. Bottcher, W. B. Dress, G. D. Alton, N. Neskovic, and C. M. Fou, Phys. Rev. Lett. **51**, 31 (1983).
[9]Y. Hahn, Phys. Rev. A **12**, 895 (1975).
[10]K. LaGattuta and Y. Hahn, Phys. Rev. Lett. **51**, 558 (1983).
[11]L. J. Roszman and A. W. Weiss, J. Quant. Spectrosc. Radiat. Transfer **30**, 67 (1983).
[12]S. M. Younger, J. Quant. Spectrosc. Radiat. Transfer **29**, 67 (1983).
[13]D. C. Griffin, M. S. Pindzola, and C. Bottcher, Phys. Rev. A **31**, 568 (1985).
[14]P. G. Burke and W. Eissner, in *Atoms in Astrophysics,* edited by P. G. Burke, W. B. Eissner, D. G. Hummer, and I. C. Percival (Plenum, New York, 1983), p. 1.
[15]A. K. Pradhan, Phys. Rev. Lett. **47**, 79 (1981).
[16]L. P. Presnyakov and R. K. Janev, in *Atomic Collision Processes with Multiply Charged Ions,* edited by B. Perovic (Boris Kidric Institute of Nuclear Sciences, Belgrade, 1983), p. 155.
[17]A. V. Vinogradov and V. N. Shlyaptsev, Kvant. Elektron. (Moscow) **7**, 1319 (1980) [Sov. J. Quantum Electron. **10**, 754 (1980)].
[18]U. Feldman, J. F. Seely, and A. K. Bhatia, J. Appl. Phys. **56**, 2475 (1984).
[19]D. L. Mathews, P. L. Hagelstein, M. D. Rosen, M. J. Eckart, N. M. Ceglio, A. U. Hazi, H. Medecki, B. J. MacGowan, J. E. Trebes, B. L. Whitten, E. M. Campbell, C. W. Hatcher, A. M. Hawryluk, R. L. Kauffman, L. D. Pleasance, G. Rambach, J. H. Scofield, G. Stone, and T. A. Weaver, Phys. Rev. Lett. **54**, 110 (1985).
[20]M. S. Pindzola, D. C. Griffin, C. Bottcher, D. C. Gregory, A. M. Howald, R. A. Phaneuf, D. H. Crandall, G. H. Dunn, D. W. Mueller, and T. J. Morgan, Oak Ridge National Laboratory Report No. ORNL/TM-9436, 1985 (unpublished).
[21]R. D. Cowan, The Theory of Atomic Structure and Spectra (University of California, Berkeley, 1981).
[22]R. D. Cowan and D. C. Griffin, J. Opt. Soc. Am. **66**, 1010 (1976).
[23]M. E. Riley and D. G. Truhlar, J. Chem. Phys. **63**, 2182 (1975).
[24]J. B. Mann (private communication).
[25]D. C. Griffin, M. S. Pindzola, and C. Bottcher, Oak Ridge National Laboratory Report No. ORNL/TM-9478, 1985 (unpublished).